Published in final edited form as:
Proteins. 2008 November 1; 73(2): 431–439. doi:10.1002/prot.22066.

Structures of a Potent Phenylalkyl Bisphosphonate Inhibitor Bound to Farnesyl and Geranylgeranyl Diphosphate Synthases

Rong Cao[1], **Cammy K.-M. Chen**[2,3], **Rey-Ting Guo**[2], **Andrew H.-J. Wang**[2], and **Eric Oldfield**[1,4]

1 *Center for Biophysics and Computational Biology, 607 South Mathews Avenue, University of Illinois at Urbana-Champaign, Urbana, Illinois 61801, USA*

2 *Institute of Biological Chemistry, Academia Sinica, 128 Academia Road, Sec 2 Nankang, Taipei, Taiwan 11529*

3 *Institute of Biochemical Sciences, National Taiwan University, Taipei 106, Taiwan*

4 *Department of Chemistry, University of Illinois at Urbana-Champaign, 600 South Mathews Avenue, Urbana, IL 61801*

Abstract

We report the x-ray crystallographic structures of the bisphosphonate N-[methyl(4-phenylbutyl)]-3-aminopropyl-1-hydroxy-1,1-bisphosphonate **(BPH-210),** a potent analog of pamidronate (Aredia), bound to farnesyl diphosphate synthase (FPPS) from *Trypanosoma brucei* as well as to geranylgeranyl diphosphate synthase from *Saccharomyces cerevisiae*. **BPH-210** binds to FPPS, together with 3 Mg^{2+}, with its long, hydrophobic phenylbutyl sidechain being located in the same binding pocket that is occupied by allylic diphosphates and other bisphosphonates. Binding is overwhelmingly entropy driven, as determined by isothermal titration calorimetry. The structure is of interest since it explains the lack of potency of longer chain analogs against FPPS, since these would be expected to have a steric clash with an aromatic ring at the distal end of the binding site. Unlike shorter chain FPPS inhibitors, such as pamidronate, **BPH-210** is also found to be a potent inhibitor of human geranylgeranyl diphosphate synthase. In this case, the bisphosphonate binds only to the GGPP product inhibitory site, with only 1 (chain A) or 0 (chain B) Mg^{2+}, and ΔS is much smaller and ΔH is ~6k cal more negative than in the case of FPPS binding. Overall, these results are of general interest since they show that some bisphosphonates can bind to more than one *trans*-prenyl synthase enzyme which, in some cases, can be expected to enhance their overall activity *in vitro* and *in vivo*.

INTRODUCTION

Bisphosphonates such as pamidronate (**1**, Aredia), risedronate (**2**, Actonel), zoledronate (**3**, Zometa) and ibandronate (**4**, Boniva) are used to treat a variety of bone resorption diseases [1, 2], and there is also current interest in the use of bisphosphonates in immunotherapy of cancer since they activate γδ T cells (containing the Vγ2Vδ2 T cell receptor) of the immune system to kill tumor cells[3,4]. In earlier work [5], we proposed that these so-called nitrogen-containing bisphosphonates acted as cationic transition state/reactive intermediate analogs, binding to the allylic substrate binding site in the enzyme farnesyl diphosphate synthase (EC 2.5.1.10). This proposal turned out to be correct, and there are currently several published x-ray crystallographic structures of bisphosphonates bound to FPPSs from a variety of organisms,

#To whom enquiries should be addressed: Email eo@chad.scs.uiuc.edu; Phone 217-333-3374; Fax 217-244-0997.

including *Escherichia coli*[6], human [7,8], *Trypanosoma cruzi*[9], *Trypanosoma brucei*[10], and *Cryptosporidium parvum*[11]. The vast majority of published structures have focused on commercially available bisphosphonates, such as those shown below. However, another particularly potent class (in bone resorption) of bisphosphonates which have not yet been investigated structurally are the "aryl-x" bisphosphonates, such as **5 (BPH-210, using our previous nomenclature)**, a very potent inhibitor from Novartis [12], containing a long (phenylbutyl) side-chain. This compound is of interest since in addition to being very active as a bone anti-resorptive agent, it is also one of the most potent bisphosphonate inhibitors of bacterial (*E. coli*) cell growth [13], as well as having low μM activity against *T. brucei* (the causative agent of African sleeping sickness), with an IC_{50} of 250 nM (K_i = 21 nM) against *T. brucei* FPPS (Yin, F., Cao, R., et al., unpublished result) and an IC_{50} = 2.4 μM in *T. brucei* cell growth inhibition (Croft, SL., et al., personal communication). Moreover, **BPH-210** has activity against *P. falciparum*[14], the causative agent of one form of malaria. There is, therefore, interest in determining how this molecule binds to FPPS from one or more of these organisms, and here we report the first x-ray crystallographic structure of **BPH-210** bound to FPPS, from *T. brucei*. We also show that, unlike most other bisphosphonates (e.g. **1-4**), **BPH-210** is also a relatively potent inhibitor of geranylgeranyl diphosphate synthase (GGPPS). In recent work, the structures of GGPPS from two species, human and *Saccharomyces cerevisiae*, have been reported[15,16] and it has been shown that, unlike FPPS, there are three possible bisphosphonate binding sites, with the most potent GGPPS inhibitors binding to the GGPPS product inhibitory site[15,16]. We investigate here the binding of **BPH-210** to the *S. cerevisiae* enzyme. In addition, we have also determined the thermodynamics of binding of **BPH-210** to both FPPS and GGPPS. While ΔG values are similar, ΔH and ΔS vary considerably, although in both cases, binding is entropy driven.

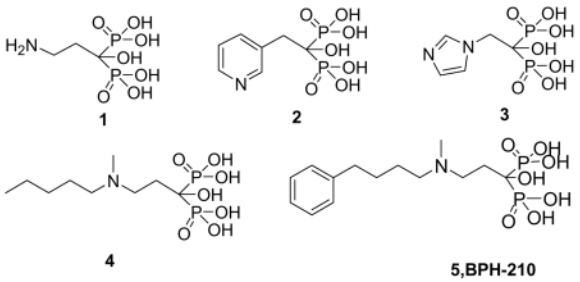

MATERIALS AND METHODS

Crystallization and data collection for *T. brucei* FPPS·BPH-210

Protein expression and crystallization were based on the crystallization conditions reported by Mao et al. [10,17]. To obtain inhibitor bound crystals, protein at 5.55 mg/mL in 10 mM Hepes, pH 7.4, 1 mM $MgCl_2$ and 10 mM mercaptoethanol was mixed with 2.5 mM **BPH-210** plus 2.5 mM $MgCl_2$, then incubated overnight on ice before setting up the drops. Crystals were grown at room temperature in hanging drops by mixing 1 μL of protein/bisphosphonate solution and 1 μL of precipitant, consisting of 10% (v/v) MPD and 100 mM ammonium acetate, pH 5.75. Prior to data collection, crystals were mounted in a cryo-loop and flash-frozen in liquid nitrogen after addition of 40% (v/v) MPD as a cryoprotectant. Diffraction data were obtained at 100 K using an ADSC Q4 CCD detector at the Advanced Photon Source, beamline 22BM (λ=1.0 Å). Diffraction data were processed and scaled by using the program HKL2000 [18]. The crystals belonged to the $P3_121$ space group, with unit cell parameters of a = b = 92.214 Å and c = 177.747 Å. Each asymmetric unit contained two FPPS molecules. Data collection statistics are shown in Table 1.

Structure determination of *T. brucei* FPPS· BPH-210

The crystal structure of *T. brucei* FPPS· **BPH-210** was determined by using the molecular replacement method using the program Molrep[19]. The previously solved *T. brucei* FPPS structure (PDB: 2EWG) [10] minus the ligand was used as a starting model. The 2Fo-Fc difference Fourier map showed clear electron densities for most amino acid residues, including those in the substrate binding site. Bisphosphonate density was obvious. Iterative rounds of refinement using CNS [20] and rebuilding using Coot [21] were then carried out. R_{free}, computed with 3% randomly selected reflections was used as a quality monitor[23]. Solvent molecules were finally added and verified from the electron density map. This yielded R/R_{free} values of 0.266/0.299. The quality of the refined model was assessed by using the Procheck[22] program. The Ramachandran plot for the structure was of good quality. Additional statistics for the final model (PDB: 2P1C) are shown in Table 1.

Crystallization and data collection for *S. cerevisiae* GGPPS• BPH-210

Crystals of GGPPS• **BPH-210** were prepared as described previously[16]. Basically, native GGPPS crystals were prepared by using the hanging drop method by mixing 2 μL of GGPPS solution with 2 μL of precipitant solution containing 0.08 M CH_3COONa, pH 4.6, 16% PEG 4000, 6–10% glycerol, and 6–10% 1, 2-propanediol. Crystals were then soaked in a cryoprotectant solution containing 2.5 mM $MgCl_2$, 2.5 mM **BPH-210**, 0.08 M CH_3COONa, pH 4.6, 20% PEG 4000, 10% glycerol, and 10% 1, 2-propanediol, for 3–12 h. X-ray diffraction data were collected at beam line BL13B1 of the National Synchrotron Radiation Research Center (NSRRC, Hsinchu, Taiwan). Diffraction data were processed and scaled by using the program HKL2000[18]. Data collection statistics are shown in Table 1. Prior to use in structural refinements, 5% randomly selected reflections were set aside for calculating R_{free} as a quality monitor[23].

Structure determination of *S. cerevisiae* GGPPS• BPH-210

The structure of GGPPS• **BPH-210** was determined by using native GGPPS (PDB: 2DH4) as the model for molecular replacement. For GGPPS• **BPH-210**, the 2Fo-Fc difference Fourier map showed clear electron densities for most amino acid residues, including those in the inhibitor binding site, but several loops and the C-terminal segments were disordered. The density for **BPH-210** was obvious. Subsequent refinement with incorporation of the cofactors and water molecules at a 1.0σ map level yielded R and R_{free} values of 0.195 and 0.271, respectively, at 2.08 Å resolution. Additional statistics for the final model (PDB: 2Z7H) are shown in Table 1.

Isothermal titration calorimetry (ITC)

ITC measurements were performed at 25°C using a MicroCal VP-ITC (MicroCal, Inc., Northampton, MA), basically as described previously[24]. For FPPS, we titrated 8 μL of a 0.3 mM ligand solution from a 250 μL syringe (rotating at 300 rpm) into the sample cell containing 1.42 mL of a 0.018 mM *T. brucei* FPPS solution. The buffer solution was 50 mM Hepes (pH 7.4) and 5 mM $MgCl_2$. The duration of injection was set to 19.2 s, and the delay between injections was 240 s. The initial delay prior to the first injection was 60 s. To derive the heat associated with each injection, the area under each heat burst curve (microcalories per second versus seconds) was determined by integration (using Origin version 5.0 software; MicroCal, Inc., Northampton, MA). Fitting to a one-site binding model gave good accord with experiment. For GGPPS, the experimental conditions were basically the same except that 0.015 mM GGPPS and 0.8 mM **BPH-210** were used. The buffer was 50 mM phosphate, pH 7.0, 1 mM $MgCl_2$, and, again, fitting to a one-site binding model gave good accord with experiment. In this instance, we used the human enzyme since this gave higher GGPPS expression levels, and

previously we showed that there was a very good correlation (R=0.9, p=0.0035) between the Ki values for inhibition of both species by bisphosphonates[16].

RESULTS

Structure of FPPS· BPH-210

We show in Figure 1A the structure of **BPH-210** bound to *T. brucei* FPPS. There are two FPPS molecules in the asymmetric unit and one molecule of **BPH-210** binds per FPPS. There are 3 Mg^{2+} bound to each FPPS, as first observed with risedronate (**2**) bound to the *E. coli* protein by Hosfield et al. [6]. The phosphonate groups make multiple contacts with these 3 Mg^{2+}, which in turn interact with Asp residues in both the first and second DDXXD repeats, as well as with neighboring Arg 112 and Lys 212, 269, as shown in the ligand interaction diagram in Figure 1B. Very similar interactions are seen in the B chain, Figure 1C. 2Fo-Fc density maps are shown in Figure 1D, E. The phenylbutyl sidechain is involved in hydrophobic contacts with, among others, A169, M106, T168 and T213, plus, the ammonium group of **BPH-210** is close to the OH group in Y216. As can be seen more clearly in Figure 2A, the phenylbutyl side-chain essentially fully occupies the GPP/FPP binding site first identified by Tarshis et al. in the avian protein [25] and, as expected, the Mg^{2+} seen in those structures (PDB: 1UBW and 1UBX) are in close spatial proximity to the Mg^{2+} seen in the FPPS• **BPH-210** structure. The positions of these Mg^{2+}, as well as the two phosphonate groups, are also very close (~0.97 Å, rmsd) to those seen with other aromatic bisphosphonate-Mg^{2+} structures, such as in zoledronate (**3**), bound to human FPPS [7,8]. In addition, the position of the positively charged (ammonium) center in **BPH-210** is likewise very close to the cationic charge centers in, e.g. the minodronate and zoledronate (Figure 2B, 2C) FPPS structures[10] (PDB: 2EWG and 1ZW5). Unlike these smaller bisphosphonates, however, **BPH-210** has a very long side-chain, and as can be seen in Figure 2C, this extends to the end of the allylic binding site pocket, where it interacts with Y99, as evidenced by the blue disc feature on Tyr99 in the ligand interaction diagram, Figure 1B, C. The *para*-carbon on the phenyl ring on the ligand is also partially solvent exposed (blue feature on the ring), as shown in Figure 1B, C, similar to the partial solvent exposure of the distal isoprene group seen in the FPPS·**FPP** structure (PDB: 1UBX).

The interaction between Tyr99 and the phenyl ring in **BPH-210** is of interest since it suggests a role for this residue in the regulation of isoprenoid diphosphate chain length elongation. As shown in Figure 3, a ClustalW[26] alignment of *T. brucei* FPPS with rat, human and avian FPPS shows that there are two conserved aromatic amino-acids 4 and 5 residues upstream of the conserved DDXXD repeats in all four proteins. In rat, human and avian FPPS, these amino-acids are both Phe, but in the *T. brucei* FPPS, they are His and Tyr. In the avian enzyme, mutation of Phe to Ala results in isoprenoid diphosphates having chain lengths > 15-carbons[25], so these Phe residues (and by analogy His, Tyr in the *T. brucei* protein) appear to act as a "wall", inhibiting chain elongation beyond C_{15} (FPP), a steric effect. A similar effect is also seen in the *Toxoplasma gondii* "FPPS", in which there is a Phe→Cys substitution in the fifth amino acid upstream of the first DDXXD motif (Figure 3), resulting in the production of the C_{20} species, GGPP[27]. This steric effect is also reflected in the ability of different bisphosphonates to inhibit bone resorption, in rats[12]. Specifically, shorter chain species (having fewer CH_2 groups attached to the phenyl ring) have slightly less activity than does **BPH-210**: 1 and 1.4 μg/kg, as opposed to 0.4 μg/kg, for bisphosphonates containing 3 and 2 CH_2 spacer groups, respectively (as opposed to the 4 in **BPH-210**), due at least in part to decreased hydrophobic stabilization in the active site of the protein. However, a much larger effect is seen on chain elongation: for the analog of **BPH-210** containing 5 CH_2 groups, the ED_{50} for bone resorption increases from 0.4 μg/kg to 20 μg/kg, and for the species with 6 CH_2 groups, the ED_{50} increases further, to 1500 μg/kg [12]. The lack of potency of the longer chain species is likely to be due, at least in part, to steric interactions with the aromatic group

(s) at the end of the binding site, plus, increased solvent accessibility of the phenyl group in the longer chain bisphosphonates would also contribute to a decrease in activity, due to unfavorable hydrophobic interactions.

Structure of GGPPS· BPH-210

We next investigated the interaction between **BPH-210** and GGPPS. In previous work, it has been shown that small nitrogen-containing bisphosphonates have potent activity (low μM IC_{50} values, low nM K_i values) against FPPS, from a variety of species[28–31]. However, these compounds (such as risedronate, **2**) have very little activity (typically ≥ 100 μM IC_{50} values) against GGPPS[32]. On the other hand, larger, more hydrophobic bisphosphonates can be potent GGPPS inhibitors[16,32], although of course if they are sufficiently large, they will not bind to the smaller binding pocket in FPPS. Since **BPH-210** is clearly much larger than **1-4**, it seemed that it might also be a GGPPS inhibitor. This turns out to be the case, and we find an IC_{50}= 4.17 μM for **BPH-210** in GGPPS inhibition, corresponding to a K_i = 115 nM, to be compared with an IC_{50} of ~200 μM (K_i ~5.6 μM) for risedronate (**2**)[32]. This "dual" activity is of course of potential interest in the context of cell based activity, where inhibitors of both FPPS and GGPPS might lead to synergistic effects.

We thus crystallized and determined the x-ray crystallographic structure of **BPH-210** bound to GGPPS. As with FPPS, there are two molecules in the unit cell (Figure 4A) and one molecule of **BPH-210** binds to each GGPPS molecule. Interestingly, the bisphosphonate does not bind to the FPP substrate site seen previously[16], rather, it binds to the GGPP product inhibitory site, first identified by Kavanagh *et al*. in human GGPPS[15], and more recently in the yeast enzyme (PDB: 2Z4V), as can be seen in the superposition (PDB: 2Z7H, 2FVI) shown in Figure 4B. And, unlike the 3 Mg^{2+} seen in the FPPS structures (with bisphosphonates present), there is only 1 Mg^{2+} present in chain A, and 0 in chain B. Protein-ligand interactions are very similar in both chains, and are illustrated in Figures 4C, D; 2Fo-Fc density maps are in Figure 4E, F. As with FPPS, there is evidence for solvent exposure of the phenyl ring on the bisphosphonate, together with a far more pronounced solvent exposure of one of the bisphosphonate groups (which interacts with Arg69, Figure 4C,D), an interaction seen also in several other bisphosphonate-GGPPS structures[16].

Protein-ligand interactions

We next consider the question of the nature of the interactions between **BPH-210** and FPPS, and GGPPS. As can be seen in Figures 1B,C and 4C,D, there are a larger number of protein-ligand contacts in the FPPS• **BPH-210** structure than in the GGPPS• **BPH-210** structure (19, 19 versus 11, 12) and, while it is not possible to quantitate the strength of these interactions from the x-ray structures alone, the much larger number of contacts seen in the FPPS structure does suggest that binding of **BPH-210** may be stronger in the case of FPPS than with GGPPS. There are also more hydrophobic interactions in the FPPS structure, and in the GGPPS• **BPH-210** structure, one phosphonate is exposed. To assess the actual thermodynamics of binding, we used isothermal titration calorimetry. The interaction between **BPH-210** and FPPS is overwhelmingly entropy driven, with $\Delta H = 4.0$ kcal mole^{-1} and $\Delta S = 49.9$ cal deg^{-1} mole^{-1} ($T\Delta S = -14.9$ kcal mole^{-1}), as shown in Figure 5A. This is very similar to the result obtained previously with ibandronate (**4**) and *T. brucei* FPPS, where we found $\Delta H = 6.03$ kcal mole^{-1} and $\Delta S = 50.9$ cal deg^{-1} mole^{-1} (at pH = 7.4) [24]. Very similar results were also seen in the human enzyme [7,8]. As can also be seen in Figure 5A, we find 0.92 moles of **BPH-210** bound per FPPS, in accord with the single site occupancy seen in the x-ray result, Figure 1.

As previously discussed in the case of ibandronate binding to FPPS, since the configurational entropy of **BPH-210** can be expected to decrease on binding to FPPS, these results indicate the key importance of hydrophobic effects, that is, water molecules which are ordered around

BPH-210 increase their entropy on movement of **BPH-210** into the FPPS active site, and ordered water molecules in the active site also increase their entropy as they transfer to the bulk solvent, on ligand binding. On the other hand, in the case of **BPH-210** binding to GGPPS, although binding is still entropy driven, binding is weaker and is exothermic, not endothermic, Figure 5B. For FPPS, we find that $\Delta G = -11$ kcal mole^{-1} while for GGPPS, we find that $\Delta G = -9.3$ kcal mole^{-1} (Figures 5A, B) with the $T\Delta S$ term (−15 kcal vs. −6.9 kcal) clearly resulting in enhanced binding to FPPS over GGPPS. This result is also consistent with our K_i values (obtained of course under different experimental conditions and in the presence of isopentenyl diphosphate and either geranyldiphosphate or farnesyl diphosphate): K_i (**BPH-210**, *T.brucei* FPPS)=21 nM and K_i (**BPH-210**, human GGPPS)=115 nM (data not shown).

CONCLUSIONS

The results we have described above are of interest since they represent the first x-ray crystallographic structures of a potent farnesyl diphosphate synthase inhibitor which also inhibits geranylgeranyl diphosphate synthase. The bisphosphonate binds exclusively to the allylic site in FPPS, with its terminal phenyl ring having a face to face interaction with Y99, in the *T. brucei* protein. This binding motif and interaction pattern helps explain why this compound is a particularly potent inhibitor in bone resorption: shorter polymethylene side-chains can be expected to have poorer hydrophobic interactions in the FPPS active site, while larger ones lose almost all activity (n=4, ED_{50} = 0.4 μg/kg; n=5, ED_{50} = 20 μg/kg; n=6, ED_{50} = 1500 μg/kg, in bone resorption, where n is the number of methylene group spacers attached to the phenyl ring), due to repulsive steric interactions with F99 (in rat FPPS), located at the end of the allylic binding site, together with energetically unfavorable increased solvent-exposure with the longer-chain species. The close proximity of the phenyl ring in **BPH-210** to residues that are likely to be involved in chain-length determination in some pathogenic species is also of interest since, with suitable functionalization, it may be possible to more specifically target these systems. In the case of GGPPS inhibition, the bisphosphonate binds exclusively to the GGPP product inhibitory site, not the FPP substrate site. There are fewer protein-ligand contacts seen in the GGPPS structure, and binding is weaker, as determined by both isothermal titration calorimetry and by Ki values, but in both enzymes, binding is still entropy driven. The ability of some bisphosphonates to inhibit both FPPS as well as GGPPS suggests that “dual function” bisphosphonates targeting more than one prenyltransferase may be worth pursuing further, since they may have enhanced activity in inhibiting protein prenylation, by inhibiting the sequential steps in the isoprenoid biosynthesis pathway.

Accession Codes

The atomic coordinates and structure factors for FPPS complexed with **BPH-210** (2P1C) and GGPPS complexed with **BPH-210** (2Z7H) have been deposited in the RCSB Protein Data Bank.

Acknowledgements

This work was supported by the United States Public Health Service (National Institutes of Health grant GM65307). We thank Roberto Docampo and Andrea Montalvetti for providing the *T. brucei* FPPS expression system and Hiroshi Sagami for providing the human GGPPS system. FPPS·**BPH-210** data were collected at the Southeast Regional Collaborative Access Team (SER-CAT) 22BM beamline at the Advanced Photon Source, Argonne National Laboratory. Use of the Advanced Photon Source was supported by the U. S. Department of Energy, Office of Science, Office of Basic Energy Sciences, under Contract No. W-31-109-Eng-38. GGPPS·**BPH-210** data were collected at National Synchrotron Radiation Research Center, a national user facility supported by the National Science Council of Taiwan, ROC (grant NSC95-3112-B-001-015-Y to AH.-J.W.).

References

1. Russell RG. Bisphosphonates: from bench to bedside. Ann N Y Acad Sci 2006;1068:367–401. [PubMed: 16831938]
2. Green JR. Bisphosphonates: preclinical review. Oncologist 2004;9 (Suppl 4):3–13. [PubMed: 15459425]
3. Kunzmann V, Bauer E, Wilhelm M. γδ T-cell stimulation by pamidronate. N Engl J Med 1999;340 (9):737–738. [PubMed: 10068336]
4. Dieli F, Vermijlen D, Fulfaro F, Caccamo N, Meraviglia S, Cicero G, Roberts A, Buccheri S, D'Asaro M, Gebbia N, Salerno A, Eberl M, Hayday AC. Targeting human γδ T cells with zoledronate and interleukin-2 for immunotherapy of hormone-refractory prostate cancer. Cancer Res 2007;67(15): 7450–7457. [PubMed: 17671215]
5. Martin MB, Arnold W, Heath HT 3rd, Urbina JA, Oldfield E. Nitrogen-containing bisphosphonates as carbocation transition state analogs for isoprenoid biosynthesis. Biochem Biophys Res Commun 1999;263(3):754–758. [PubMed: 10512752]
6. Hosfield DJ, Zhang Y, Dougan DR, Broun A, Tari LW, Swanson RV, Finn J. Structural basis for bisphosphonate-mediated inhibition of isoprenoid biosynthesis. J Biol Chem 2004;279(10):8526–8529. [PubMed: 14672944]
7. Kavanagh KL, Guo K, Dunford JE, Wu X, Knapp S, Ebetino FH, Rogers MJ, Russell RG, Oppermann U. The molecular mechanism of nitrogen-containing bisphosphonates as antiosteoporosis drugs. Proc Natl Acad Sci USA 2006;103(20):7829–7834. [PubMed: 16684881]
8. Rondeau JM, Bitsch F, Bourgier E, Geiser M, Hemmig R, Kroemer M, Lehmann S, Ramage P, Rieffel S, Strauss A, Green JR, Jahnke W. Structural basis for the exceptional *in vivo* efficacy of bisphosphonate drugs. ChemMedChem 2006;1(2):267–273. [PubMed: 16892359]
9. Gabelli SB, McLellan JS, Montalvetti A, Oldfield E, Docampo R, Amzel LM. Structure and mechanism of the farnesyl diphosphate synthase from *Trypanosoma cruzi*: implications for drug design. Proteins 2006;62(1):80–88. [PubMed: 16288456]
10. Mao J, Mukherjee S, Zhang Y, Cao R, Sanders JM, Song Y, Meints GA, Gao YG, Mukkamala D, Hudock MP, Oldfield E. Solid-state NMR, crystallographic, and computational investigation of bisphosphonates and farnesyl diphosphate synthase-bisphosphonate complexes. J Am Chem Soc 2006;128(45):14485–14497. [PubMed: 17090032]
11. Vedadi M, Lew J, Artz J, Amani M, Zhao YDA, Wasney GAGM, Hills T, Brokx S, Qiu W, Sharma S, Diassiti A, Alam Z, Melone M, Mulichak A, Wernimont A, Bray J, Loppnau P, Plotnikova O, Newberry K, Sundararajan E, Houston S, Walker J, Tempel W, Bochkarev A, Kozieradzki I, Edwards A, Arrowsmith C, Roos D, Kain K, Hui R. Cryptosporidium parvum putative polyprenyl pyrophosphate synthase (cgd4_2550) in complex with zoledronate PDB 2HER. 2006
12. Widler L, Jaeggi KA, Glatt M, Muller K, Bachmann R, Bisping M, Born AR, Cortesi R, Guiglia G, Jeker H, Klein R, Ramseier U, Schmid J, Schreiber G, Seltenmeyer Y, Green JR. Highly potent geminal bisphosphonates. From pamidronate disodium (Aredia) to zoledronic acid (Zometa). J Med Chem 2002;45(17):3721–3738. [PubMed: 12166945]
13. Leon A, Liu L, Yang Y, Hudock MP, Hall P, Yin F, Studer D, Puan KJ, Morita CT, Oldfield E. Isoprenoid biosynthesis as a drug target: bisphosphonate inhibition of *Escherichia coli* K12 growth and synergistic effects of fosmidomycin. J Med Chem 2006;49(25):7331–7341. [PubMed: 17149863]
14. Ghosh S, Chan JM, Lea CR, Meints GA, Lewis JC, Tovian ZS, Flessner RM, Loftus TC, Bruchhaus I, Kendrick H, Croft SL, Kemp RG, Kobayashi S, Nozaki T, Oldfield E. Effects of bisphosphonates on the growth of *Entamoeba histolytica* and *Plasmodium* species *in vitro* and *in vivo*. J Med Chem 2004;47(1):175–187. [PubMed: 14695831]
15. Kavanagh KL, Dunford JE, Bunkoczi G, Russell RG, Oppermann U. The crystal structure of human geranylgeranyl pyrophosphate synthase reveals a novel hexameric arrangement and inhibitory product binding. J Biol Chem 2006;281(31):22004–22012. [PubMed: 16698791]
16. Guo RT, Cao R, Liang PH, Ko TP, Chang TH, Hudock MP, Jeng WY, Chen CK, Zhang Y, Song Y, Kuo CJ, Yin F, Oldfield E, Wang AH. Bisphosphonates target multiple sites in both *cis*- and *trans*-prenyltransferases. Proc Natl Acad Sci USA 2007;104(24):10022–10027. [PubMed: 17535895]

17. Mao J, Gao YG, Odeh S, Robinson H, Montalvetti A, Docampo R, Oldfield E. Crystallization and preliminary X-ray diffraction study of the farnesyl diphosphate synthase from *Trypanosoma brucei*. Acta Crystallogr D Biol Crystallogr 2004;60(Pt 10):1863–1866. [PubMed: 15388934]
18. Otwinowski Z, Minor W. Processing of X-ray diffraction data collected in oscillation mode. Methods in Enzymology 1997;276:307–326.
19. Vagin A, Teplyakov A. An approach to multi-copy search in molecular replacement. Acta Crystallogr D Biol Crystallogr 2000;56(Pt 12):1622–1624. [PubMed: 11092928]
20. Brunger AT, Adams PD, Clore GM, DeLano WL, Gros P, Grosse-Kunstleve RW, Jiang JS, Kuszewski J, Nilges M, Pannu NS, Read RJ, Rice LM, Simonson T, Warren GL. Crystallography & NMR system: A new software suite for macromolecular structure determination. Acta Crystallogr D Biol Crystallogr 1998;54(Pt 5):905–921. [PubMed: 9757107]
21. Emsley P, Cowtan K. Coot: model-building tools for molecular graphics. Acta Crystallogr D Biol Crystallogr 2004;60(Pt 12 Pt 1):2126–2132. [PubMed: 15572765]
22. Laskowski RA, MacArthur MW, Moss DS, Thornton JM. PROCHECK: a program to check the stereochemical quality of protein structures. J Appl Crystallogr 1993;26:283–291.
23. Brunger AT. Assessment of Phase Accuracy by Cross Validation - the Free R-Value - Methods and Applications. Acta Crystallogr D Biol Crystallogr 1993;49:24–36. [PubMed: 15299543]
24. Yin F, Cao R, Goddard A, Zhang Y, Oldfield E. Enthalpy versus entropy-driven binding of bisphosphonates to farnesyl diphosphate synthase. J Am Chem Soc 2006;128(11):3524–3525. [PubMed: 16536518]
25. Tarshis LC, Proteau PJ, Kellogg BA, Sacchettini JC, Poulter CD. Regulation of product chain length by isoprenyl diphosphate synthases. Proc Natl Acad Sci USA 1996;93(26):15018–15023. [PubMed: 8986756]
26. Thompson JD, Higgins DG, Gibson TJ. CLUSTAL W: improving the sensitivity of progressive multiple sequence alignment through sequence weighting, position-specific gap penalties and weight matrix choice. Nucleic Acids Res 1994;22(22):4673–4680. [PubMed: 7984417]
27. Ling Y, Li ZH, Miranda K, Oldfield E, Moreno SN. The farnesyl-diphosphate/geranylgeranyl-diphosphate synthase of *Toxoplasma gondii* is a bifunctional enzyme and a molecular target of bisphosphonates. J Biol Chem 2007;282(42):30804–30816. [PubMed: 17724033]
28. Grove JE, Brown RJ, Watts DJ. The intracellular target for the antiresorptive aminobisphosphonate drugs in *Dictyostelium discoideum* is the enzyme farnesyl diphosphate synthase. J Bone Miner Res 2000;15(5):971–981. [PubMed: 10804029]
29. Montalvetti A, Fernandez A, Sanders JM, Ghosh S, Van Brussel E, Oldfield E, Docampo R. Farnesyl pyrophosphate synthase is an essential enzyme in *Trypanosoma brucei. In vitro* RNA interference and *in vivo* inhibition studies. J Biol Chem 2003;278(19):17075–17083. [PubMed: 12618430]
30. Montalvetti A, Bailey BN, Martin MB, Severin GW, Oldfield E, Docampo R. Bisphosphonates are potent inhibitors of *Trypanosoma cruzi* farnesyl pyrophosphate synthase. J Biol Chem 2001;276(36): 33930–33937. [PubMed: 11435429]
31. Dunford JE, Thompson K, Coxon FP, Luckman SP, Hahn FM, Poulter CD, Ebetino FH, Rogers MJ. Structure-activity relationships for inhibition of farnesyl diphosphate synthase *in vitro* and inhibition of bone resorption *in vivo* by nitrogen-containing bisphosphonates. J Pharmacol Exp Ther 2001;296 (2):235–242. [PubMed: 11160603]
32. Szabo CM, Matsumura Y, Fukura S, Martin MB, Sanders JM, Sengupta S, Cieslak JA, Loftus TC, Lea CR, Lee HJ, Koohang A, Coates RM, Sagami H, Oldfield E. Inhibition of geranylgeranyl diphosphate synthase by bisphosphonates and diphosphates: a potential route to new bone antiresorption and antiparasitic agents. J Med Chem 2002;45(11):2185–2196. [PubMed: 12014956]

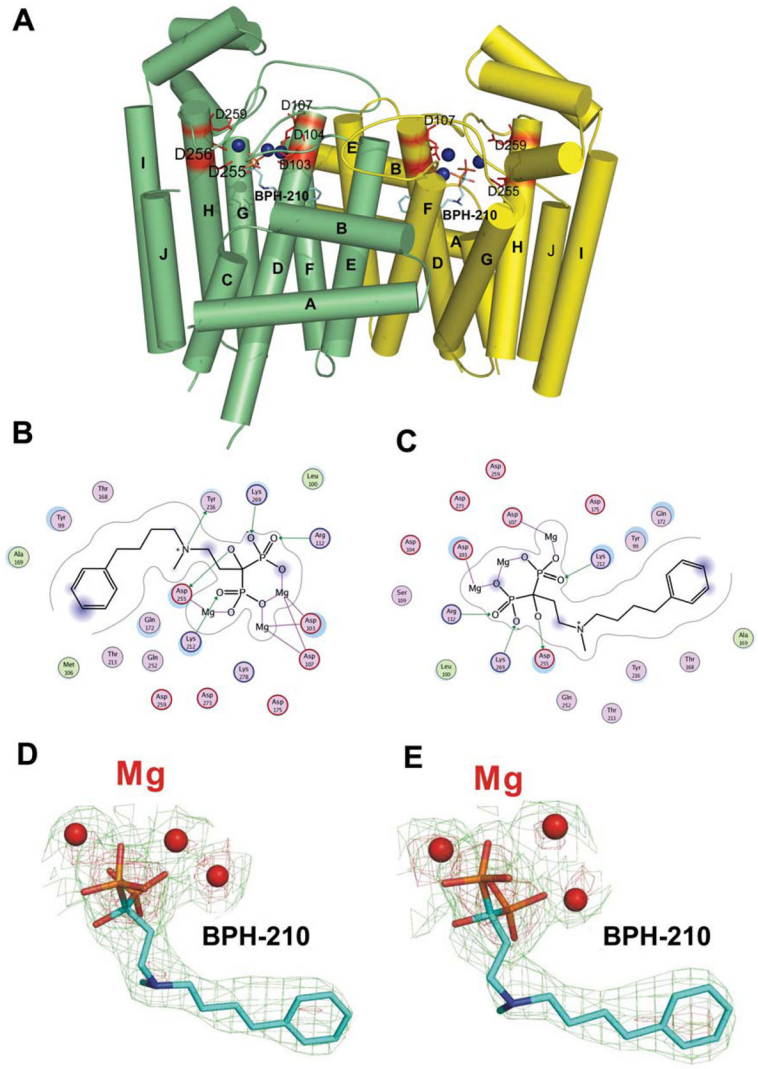

Fig. 1.

Structure and interactions in FPPS• **BPH-210**. (**A**) Schematic of *T. brucei* FPPS• **BPH-210** dimer. **(B)** Ligplot interaction diagram show FPPS• **BPH-210** interactions in chain A. **(C)** Ligplot interaction diagram of FPPS• **BPH-210** interactions in chain B. **(D)** 2Fo-Fc electron density map for **BPH-210** bound to FPPS in chain A (green contoured at 1σ, red at 3σ). **(E)** 2Fo-Fc electron density map for **BPH-210** in chain B (green contoured at 1σ, red at 3σ).

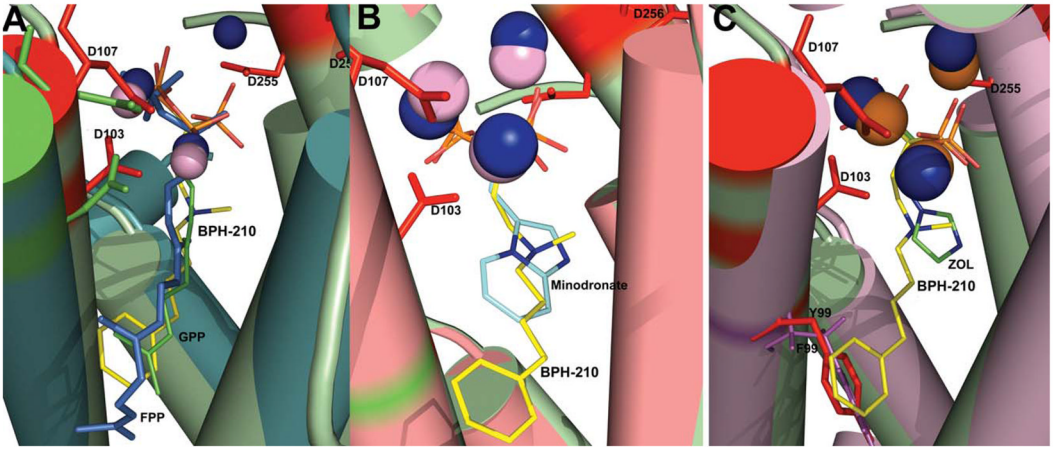

Fig. 2.

Comparison of FPPS• **BPH-210** and other FPPS structures. **(A)** superimposed structures of *T. brucei* FPPS• **BPH-210** with avian FPPS containing GPP or FPP (PDB: 1UBX, 1UBW). **BPH-210** is in yellow; GPP, green, FPP, blue. The 3 Mg^{2+} in the *T. brucei* FPPS structure are in dark blue, the Mg^{2+} in the avian FPPS structures are in pink. **(B)** *T. brucei* FPPS• **BPH-210** structure as in **A** (same colors) superimposed on *T. brucei* minodronate (PDB: 2EWG)-FPPS structure (minodronate in blue, Mg^{2+} in this structure in pink). **(C)** *T. brucei* FPPS• **BPH-210** structure (colors as in **A**) superimposed on human zoledronate FPPS complex; PDB: 1ZW5) (zoledronate, blue; Mg^{2+} in this structure in pink). Also shown is the close proximity between Y99 (red) in the *T. brucei* structure and F99 (purple) in the human structure.

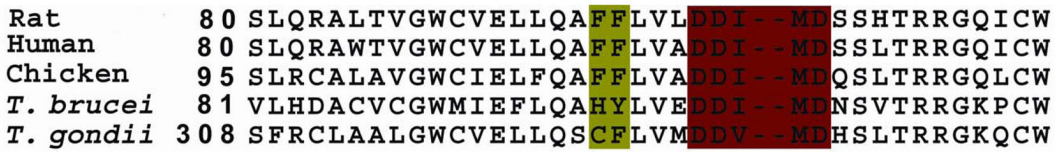

Fig. 3.

Partial sequence alignment of rat, human, chicken, *T. brucei*, *T. gondi*, FPPSs. The "first DDXXD" repeat is shaded in red, the two aromatic amino-acids 4 and 5 residues upstream of the first DDXXD repeat (PhePhe in rat, human and chicken, HisTyr in *T. brucei*) that control to a significant extent, product specificity, and which are likely to interact with the phenyl ring in **BPH-210,** are shown in green.

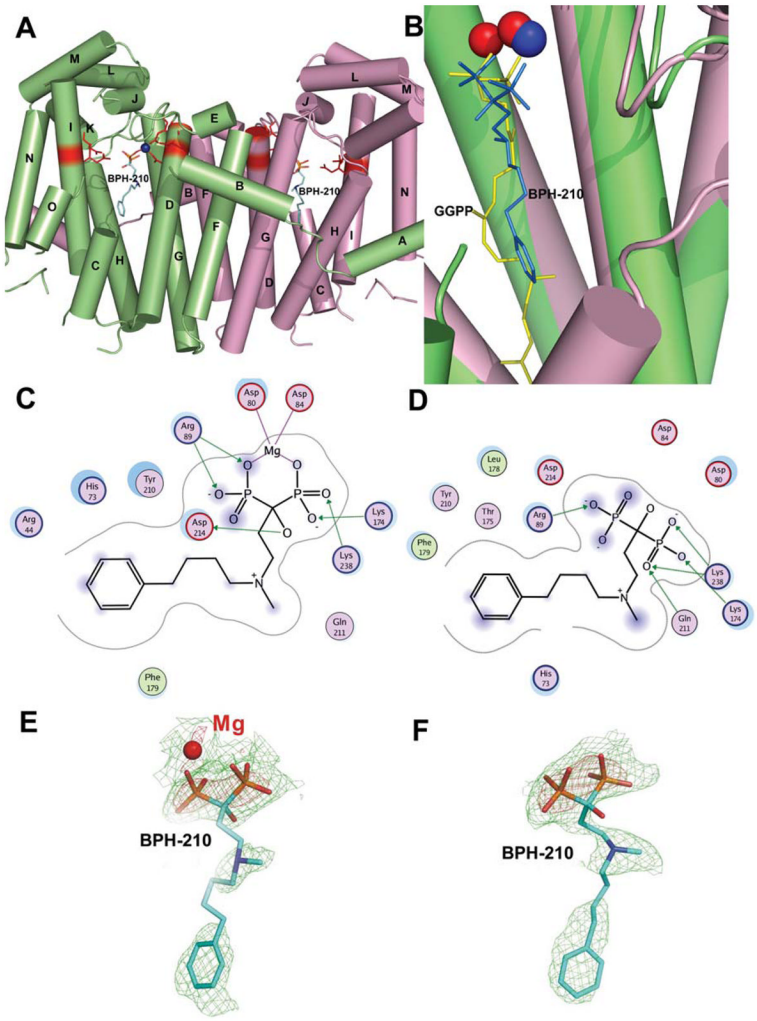

Fig. 4.

Structures and interactions in GGPPS·**BPH-210. (A)** Structure of GGPPS·**BPH-210. (B)** Close-up view of GGPPS·**BPH-210** (in blue, PDB: 2Z7H) superimposed on human GGPPS with bound GGPPS (yellow; PDB: 2FVI). The Mg^{2+} in the *S. cerevisae* GGPPS·**BPH-210** structure is in blue, the Mg^{2+} in the human GGPPS•GGPP structure, in red. **(C)** Ligplot interactions in chain A of the GGPPS·**BPH-210** complex. **(D)** Ligplot interactions in chain B. **(E)** 2Fo-Fc electron density map for **BPH-210** bound to GGPPS in chain A (green contoured at 1σ, red at 3σ). **(F)** 2Fo-Fc electron density map for **BPH-210** in chain B (green contoured at 1σ, red at 3σ).

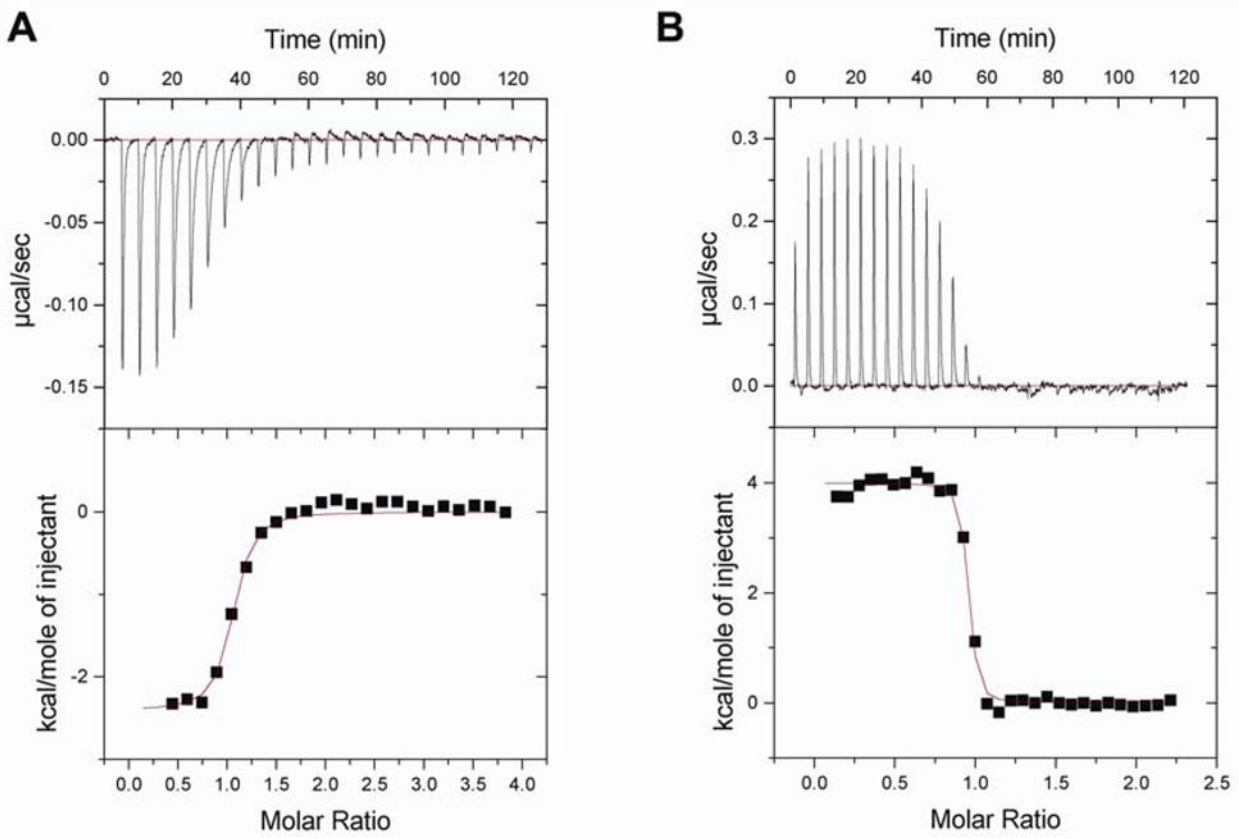

Fig. 5.

Isothermal titration calorimetry results. **(A)** ITC results at 300K for **BPH-210** binding to *T. brucei* FPPS. Binding is overwhelmingly entropy driven ($\Delta H = 4.0$ kcal mole^{-1}, $\Delta S = 49.9$ cal deg^{-1} mole, $-T\Delta S = 14.9$ kcal mole^{-1}, Chi^2 =67712) and n=0.92. **(B)** ITC results at 300K for **BPH-210** binding to *H. sapiens* GGPPS. Binding is enthalpy driven ($\Delta H = -2.41$ kcal mole^{-1}, $\Delta S = 23.07$ cal deg^{-1} mole^{-1}, $-T\Delta S = 6.92$ kcal mole^{-1}, Chi^2 =7595) and n = 1.00.

Table 1

Data collection and refinement statistics for **BPH-210**, N-[methyl(4-phenylbutyl)]-3-aminopropyl-1-hydroxy-1,1-bisphosphonate, bound to *T. brucei* FPPS (2P1C) and *S. cerevisiae* GGPPS (2Z7H).

PDB number	2P1C	2Z7H
Data collection		
Space group	$P3_121$	$P2_12_12_1$
Unit cell		
α=β (°)	90,	90
γ (°)	120	90
a (Å)	92.124	47.41
b (Å)	92.124	116.64
c (Å)	177.747	128.14
X-ray source	APS-22BM[a]	NSSRC-BL13B1[c]
Resolution (Å)	30-2.37 (2.45–2.37)	30-2.08 (2.15–2.08)
No. of reflection observed	315,360	213,350
Unique	34,615 (2,457)	77,404 (7152)
Completeness (%)	95.7 (69.7)	94.3 (89.5)
R-merge	0.087 (0.664)	0.045 (0.287)
$I/\sigma I$	24.3	30.9
Multiplicity	9.1 (5.1)	5.2 (4.7)
Refinement statistics		
Resolution range (Å)	30.0–2.45 (2.54–2.45)	30.0–2.08 (2.15–2.08)
R-work/*R*-free (%)	26.6/29.9	19.5/27.1
RMSD		
Bond lengths	0.006	0.015
Bond angles	1.100	1.600
No. of atoms		
Protein	5,704	4955
Bisphosphonates	48	48
Magnesium ion	6	1
Solvent (water)	306	633
B average (Å^2) of protein	53.70	42.9
B average (Å^2) of solvents	51.77	60.3
B average (Å^2) of ligands (bisphosphonates, Mg^{2+})	45.46	57.3
Ramachandran plot (%)		
Most favored	91.6	96.1
Additionally allowed	8.4	3.9
Generously allowed	0	0

[a] Advanced Photon Source at the Argonne National Laboratory

[b] Values in parentheses are for the highest resolution shell

[c] National Synchrotron Radiation Research Center (NSRRC, Hsinchu, Taiwan)